

pubs.acs.org/journal/ascecg Research Article

# Fabrication of Robust Paper-Based Electronics by Adapting Conventional Paper Making and Coupling with Wet Laser Writing

Cheng Wang, Zhiling Zhao, Rui Wu, Xiaowen Shi, Gregory F. Payne,\* and Xiaohui Wang\*



Cite This: ACS Sustainable Chem. Eng. 2023, 11, 9782-9791



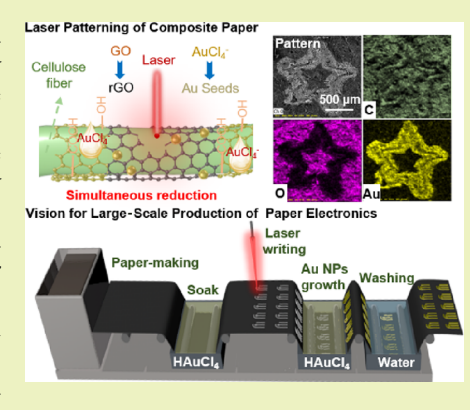
**ACCESS** I

Metrics & More

Article Recommendations

SI Supporting Information

ABSTRACT: Paper offers the potential as a sustainable substrate for electronics, yet a key remaining challenge is patterning. While most demonstration studies pattern by printing conducting inks onto cellulose, we adapt conventional paper making to create a stable non-conducting composite of graphene oxide (GO; 30%) and cellulose (70%) and then pattern this composite using wet laser writing. Specifically, the GO/cellulose composite is as follows: soaked in a HAuCl<sub>4</sub> solution; laser patterned to simultaneously reduce GO (rGO) and generate metallic gold seeds (typical writing speed 20 s·cm<sup>-2</sup>); and then incubated (30 min) in HAuCl<sub>4</sub> solution to "grow" gold nanoparticles (Au NPs) in the pre-seeded patterned region. Various methods demonstrate that laser patterning induces spatially selective chemical changes in the composite. Functionally, the patterned region (Au NPs/rGO/cellulose) shows a 200-fold increase in conductivity (1362 S m<sup>-1</sup>) compared to the unpatterned region (GO/cellulose). As a simple demonstration, we fabricated patterned composite paper electrodes and demonstrate excellent electrochemical sensing performance in terms of sensitivity,



selectivity, stability, and repeatability. We envision that laser patterning of composite paper offers unprecedented opportunities for scalable manufacturing because conventional papermaking can generate the stable substrate and laser patterning can be extended from serial writing to parallel photolithographic methods common in electronics fabrication.

KEYWORDS: cellulose paper electronics, laser patterning, graphene oxide, gold nanoparticle growth, electrochemical sensing

## ■ INTRODUCTION

Increasingly, paper is viewed as a technology platform for the development of a sustainable electronics economy due to the advantages such as low cost, light weight, easy availability, flexibility, and biodegradability. <sup>1-6</sup> Various demonstrations have reported paper-based electronics for a broad range of applications that include electrochemical sensors, strain sensors, transistors and circuits, energy storage, and human—computer interfacing. <sup>7-13</sup> While these reports demonstrate exciting opportunities, challenges remain in the large-scale fabrication of reliable high-performance paper.

The key challenge for the scalable manufacturing of paper-based electronics is the precise patterning of conducting and non-conducting regions. The "traditional" approach to patterned paper is to start with a non-conducting paper substrate and print functional materials (i.e., inks) that confer conductivity. Such printing has been realized in many labs and successfully demonstrated the exciting opportunities for patterned paper in a range of applications. There are concerns, however, associated with the reliability of printing in actual manufacturing, the stability of the paper substrate and printed pattern, and the reproducibility in the performance of such print-patterned papers. An emerging alternative approach is to adapt traditional paper manufacturing methods to generate a homogeneous composite paper that serves as a

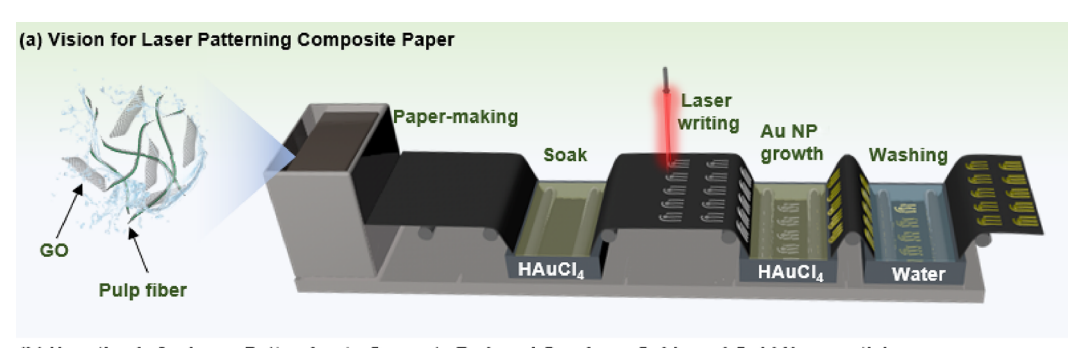
stable substrate for subsequent patterning of the conducting regions. Previous studies indicate that such composite paper can be manufactured reliably with the resulting conducting paper being stable and reproducible. The limitation is that the composite conducting paper is unpatterned and paper-cutting was needed to exert spatial control. <sup>29,30</sup>

Here, we report a potentially scalable method to pattern composite paper without printing. Figure 1a illustrates our vision that traditional paper manufacturing can be modified to generate a composite paper composed of graphene oxide (GO) and cellulose, and this composite paper can be patterned using an in-line laser patterning step. Figure 1b provides a schematic illustration of the underlying hypothesis of our patterning approach. Specifically, we provide evidence for the hypothesis that laser irradiation can be used for patterning by both converting GO to reduced GO (rGO) and by inducing the nucleation of gold "seeds" that can be subsequently grown into metallic gold nanoparticles. Previous studies have shown

Received: March 31, 2023 Revised: June 4, 2023 Published: June 16, 2023







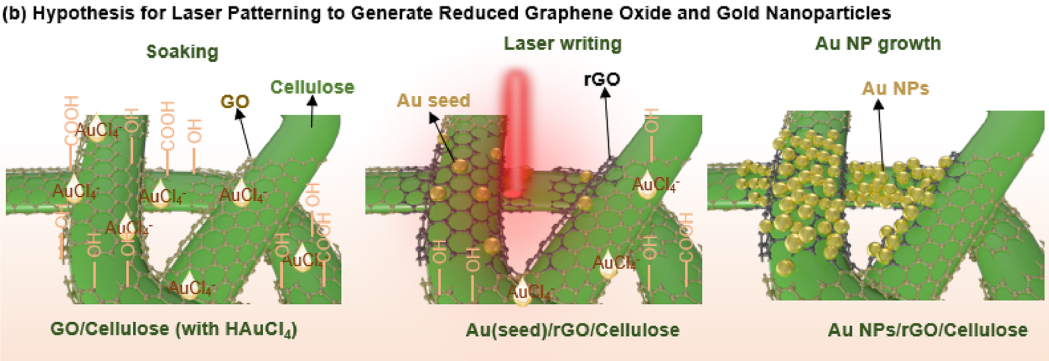


Figure 1. Vision for scalable fabrication of electronic paper. (a) Conventional paper making can be adapted to make a non-conducting composite of graphene oxide (GO) and cellulose substrate, while wet laser writing can be used to pattern conducting regions. (b) Proposed mechanism in which laser writing both removes oxygen-containing functional groups from GO to generate reduced GO (rGO) and converts HAuCl<sub>4</sub> into metallic gold seeds that can be subsequently grown into Au nanoparticles (Au NPs).

that laser writing can produce a variety of nanometals,<sup>31</sup> and we use gold in our studies because of its good electrochemical activity. As a proof of concept, we demonstrate that this patterned composite paper offers superior capabilities for electrochemical detection.

## **■ EXPERIMENTAL SECTION**

**Materials.** GO (piece of diameter 20 μm, thickness < 5 nm) was purchased from Xiwang Company (Shanghai, China). Cellulose pulp (poplar chemical pulp) was purchased from Huatai Paper Industry Co., Ltd. (Dongying, China). Cationic polyacrylamide (CPAM) was purchased from Tianjin Zhiyuan Chemical Reagent Co., Ltd. (Tianjin, China). Ag/AgCl ink was purchased from Shanghai Longsheng Co., Ltd. (Shanghai, China). Phosphate buffer solution (pH 7), hydrogen peroxide, HAuCl<sub>4</sub>·3H<sub>2</sub>O, and other chemicals were purchased from Sigma-Aldrich. All reagents were used as received without further purification. Ultrapure water (>18 MΩ) prepared by Super Milli-Q water system was used for experiments.

**Fabrication of GO/Cellulose Paper.** In initial studies, we observed that while increases in the GO content could improve the paper's conductivity, it also reduced the water filtration efficiency during the paper making process. The maximum amount of GO in the optimized composite paper is approximately 50%. Here, we adapted our previously reported method for preparing GO/cellulose paper. The procedure is as follows: a 0.5% GO slurry in water was obtained after 1 h ultrasonic treatment with a cell crusher; preparation of mixed pulp: softwood pulp was added and then 2 mL of 1% cationic polyamide was added and stirred until the water became clear; finally, this mixed pulp was poured into the Kaiser paper making machine (RK3AKWT, Austria) and diluted with 5 L of water, for the GO/cellulose paper making.

Fabrication of Au/rGO/Cellulose Paper-Based Electrochemical Sensors. For the fabrication of Au/rGO/cellulose paper, the GO/cellulose paper was soaked in 1% chloroauric acid solution for 10 min. Then, it was taken out and placed on the glass plate of the laser writing machine. The laser direct writing was started on the GO/cellulose paper according to the pattern program. The output power

of the laser (wavelength is 405 nm) was 0.6 W, and the writing speed was 20 s·cm<sup>-2</sup>. The paper after laser writing was immersed in 1% chloroauric acid solution for 30 min. The laser-patterned area of the paper electrode changes from gray to golden, which indicates that the Au/rGO/cellulose paper electrode has been successfully prepared. After coating the reference electrode with Ag/AgCl ink, the paper electrode was placed in an 80 °C oven for 20 min to obtain the Au/rGO/cellulose paper-based electrochemical sensor. The preparation of the Au/cellulose paper-based electrochemical sensor is the same as the above method, but we replace GO/cellulose paper with filter paper. In the filter paper, we need laser writing five times and grow gold nanoparticles seven times.

**Electrochemical Measurement.** Cyclic voltammetry (CV) experiments were performed under scan rates of 10, 20, 50, 100, and 150 mV s<sup>-1</sup>, respectively, and a potential range between -0.2 and 0.7 V was used. 1 M KCl was used as a supporting electrolyte for 5 mM K<sub>3</sub>Fe(CN)<sub>6</sub> solution. Electrochemical impedance spectroscopy was performed in a 5 mM K<sub>3</sub>Fe(CN)<sub>6</sub>/K<sub>4</sub>Fe(CN)<sub>6</sub> solution, and a frequency range of 100 kHz to 0.01 Hz was selected.

**Électrochemical Sensing.** Hydrogen peroxide  $(H_2O_2)$  was detected by electrochemical sensing in phosphate buffer (pH 7). The sensitivity and selectivity of the Au/rGO/cellulose paper-based electrochemical sensor for  $H_2O_2$  were measured by chronoamperometry (i-t), which was run for 20 min at a constant potential -0.25 V.

## **■ RESULTS AND DISCUSSION**

Laser Patterning to Simultaneously Reduce GO and Generate Gold Seeds. Figure 2a illustrates our hypothesis for the wet laser writing method. Initially, the GO/cellulose composite is soaked in a solution of HAuCl<sub>4</sub> (1%) and the wet paper is then irradiated to both remove oxygen-containing substituents from GO to form rGO and induce HAuCl<sub>4</sub> to form metallic gold "seeds" (the gold "seed" is small Au NPs with the size of <100 nm; see Figure S2 for further information). In a separate step, these seeds can then be grown into Au nanoparticles (NPs) by soaking in an aqueous

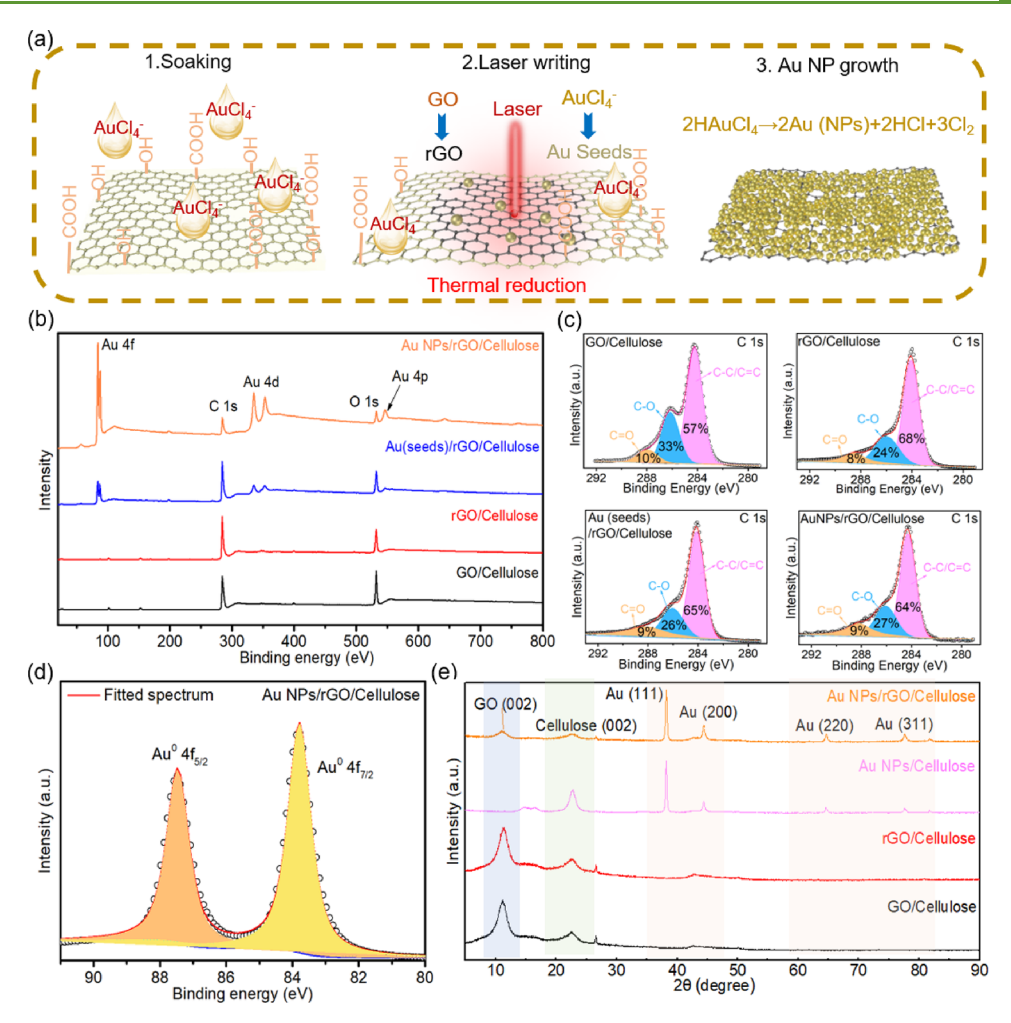


**Figure 2.** Chemical characterization. (a) Wet laser direct writing and subsequent Au nanoparticle (NP) growth are used to confer conductivity to GO/cellulose composite paper. Chemical evidence for the formation of rGO and Au NPs includes (b) X-ray photoelectron spectroscopy (XPS), (c) high-resolution XPS in the C 1s region, (d) high-resolution XPS in the Au 4f region, and (e) X-ray diffraction (XRD).

 $\rm HAuCl_4$  solution.  $^{32,33}$  To provide evidence for this hypothesis, we adapted standard paper making procedures to make a GO/cellulose composite paper from GO (30%) and cellulose (70%) and cut this composite into several specimens. Each specimen was soaked in an aqueous solution with or without  $\rm HAuCl_4$  (1%), and then the wet paper was written using a 405 nm laser (the laser-induced reactions only require irradiation for seconds; however, the writing process required a 20 s·cm $^{-2}$  pattern).

Initial characterization of these specimens was performed using XPS, as shown in Figure 2b. A comparison of the highresolution spectra in the C 1s region for the GO/cellulose composite paper before laser irradiation and after irradiation (designated rGO/cellulose) is shown in Figure 2c. These spectra show a decrease in the C=O and C-O peak areas after laser irradiation, which is consistent with the removal of oxygen-containing substituents from GO to generate rGO (additional Raman spectra are shown in Figure S1 of the Supporting Information.) The low-resolution spectra in Figure 2b shows peaks characteristic of Au when laser irradiation of the GO/cellulose composite was performed after soaking in HAuCl<sub>4</sub> solution (this specimen is designated Au(seed)/rGO/ cellulose). This observation is consistent with the formation of a gold seed upon laser irradiation. When a composite specimen was irradiated in the presence of HAuCl<sub>4</sub> and then

subsequently soaked in  $HAuCl_4$  solution (1%, 30 min) to allow the seeds to grow into Au NPs, Figure 2b suggests that the specimen has a higher content of gold. The high-resolution XPS spectrum in the Au 4f region shown in Figure 2d shows the presence of zero-valence metallic gold.<sup>34</sup> These XPS results in Figure 2c provide initial evidence that laser irradiation of the GO/cellulose composite paper can convert GO into GO and also generate metallic gold.

These specimens were also analyzed by X-ray diffraction (XRD). In addition to the above specimens, we soaked the filter paper with HAuCl<sub>4</sub> and then irradiated it with laser and grew the gold nanoparticles to obtain Au NP/cellulose specimens as the control sample (note: the patterning of cellulose specimens lacking GO is inefficient, and both the laser-writing and NP-growth steps were repeated multiple times to generate observable patterns). Figure 2e shows that the Au NP/rGO/cellulose specimen and Au NP/cellulose specimen have the characteristic peaks for Au(111), Au(200), Au(220), and Au(311).<sup>35</sup> This illustrates that the preparation of Au NPs on the paper substrate is independent of GO. These results are consistent with those from XPS and provide evidence for the successful incorporation of metallic gold into our composite paper.

Spatially Selective Au NP Growth on Pre-Seeded Composite Paper. The above results indicate that laser

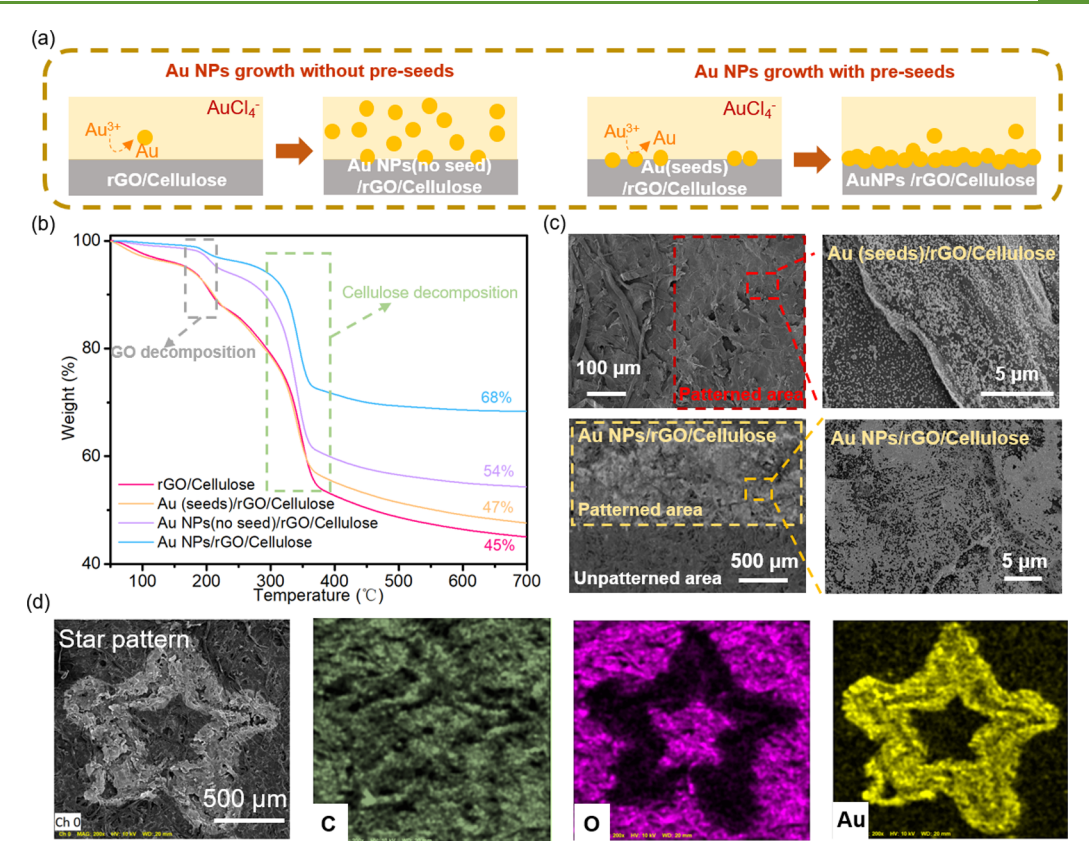


Figure 3. Pattern emergence. (a) Schematic of Au-NP growth on the laser-patterned region that had been pre-seeded with metallic gold. (b) Thermogravimetric analysis (TGA) indicates preferential NP-growth on the pre-seeded composite. (c) Scanning electron microscope (SEM) images show preferential NP growth on the patterned area. (d) Elemental analysis from energy-dispersive spectroscopy shows spatially selective removal of oxygen and Au-NP growth in the laser-patterned areas.

irradiation both converts GO to rGO and generates gold seeds, and we next demonstrated the importance of pre-seeding on the subsequent growth of Au-NPs. As illustrated schematically in Figure 3a, we visually observed that when Au-NP growth was performed with the unseeded specimen, considerably more NPs were observed to form in the growth solution compared to the specimen that had been pre-seeded with Au. To quantitatively estimate the importance of pre-seeding, we performed thermogravimetric analysis (TGA). Specifically, Figure 3b shows small differences in residual mass (45 vs 47%) when specimens of the GO/cellulose composite were laser irradiated without HAuCl<sub>4</sub> (designated rGO/cellulose) or with HAuCl<sub>4</sub> that is needed to form gold seeds (designated Au(seed)/rGO/cellulose). In contrast, when laser-irradiated specimens were immersed in HAuCl<sub>4</sub> solution to allow Au NP growth, the unseeded specimen (designated Au(no seed)/ rGO/cellulose) showed significantly less residual mass compared to the pre-seeded Au(seed)/rGO/cellulose specimen (54 vs 68%). Thus, the TGA results in Figure 3b indicate that pre-seeding the composite paper by laser irradiation in the presence of HAuCl<sub>4</sub> enhances the subsequent generation of metallic gold nanoparticles.

Further evidence for the importance of seeding is provided by the SEM images in Figure 3c. The upper left image in Figure 3c for the region of the specimen that was not laser irradiated (i.e., the unpatterned region) shows cellulose fibers, while the laser-irradiated patterned region appears smooth with no obvious fibers. The higher-resolution image at the upper right in Figure 3c shows that gold nanoparticles are evenly distributed across the surface of the patterned region

consistent with the conversion of HAuCl<sub>4</sub> into Au NP seeds.<sup>36</sup> The SEM images at the bottom in Figure 3c show the specimen after the NP growth step. The bottom-left image in Figure 3c shows a clear boundary between the patterned region (rich in Au NPs) and the unpatterned region (few Au NPs are observed). The high-resolution image at the bottom right shows the formation of an extensive network of interconnected gold NPs that preferentially grew in the previously seeded region<sup>37,38</sup> (the sizes of Au seeds and Au NPs are shown in Figure S2). Interestingly, as discussed below, it appears that the rGO in the patterned region synergistically promotes the growth of Au NPs. Ultraviolet photoelectron spectroscopy (UPS) results in Figure S3 of the Supporting Information suggests that differences in redox potential may facilitate the flow of electrons from rGO and HAuCl4 to accelerate NP growth.

To more clearly illustrate the spatially localized chemical changes that are induced by laser patterning, we patterned a GO/cellulose composite with a star (this patterned region is expected to be AuNPs/rGO/cellulose). After patterning and Au-NP growth, we analyzed the spatial distribution of the C, O, and Au elements by energy-dispersive spectroscopy (EDS). Figure 3d shows that the distribution of C is very uniform with little difference between the patterned and unpatterned regions. In contrast, the patterned region is depleted in the O element, which is consistent with the laser-induced removal of oxygenated substituents from GO. In addition, Figure 3d shows a high content of Au in the patterned region consistent with a laser-induced seeding of Au and a subsequent spatially selective growth of Au NPs onto the pre-seeded regions. As

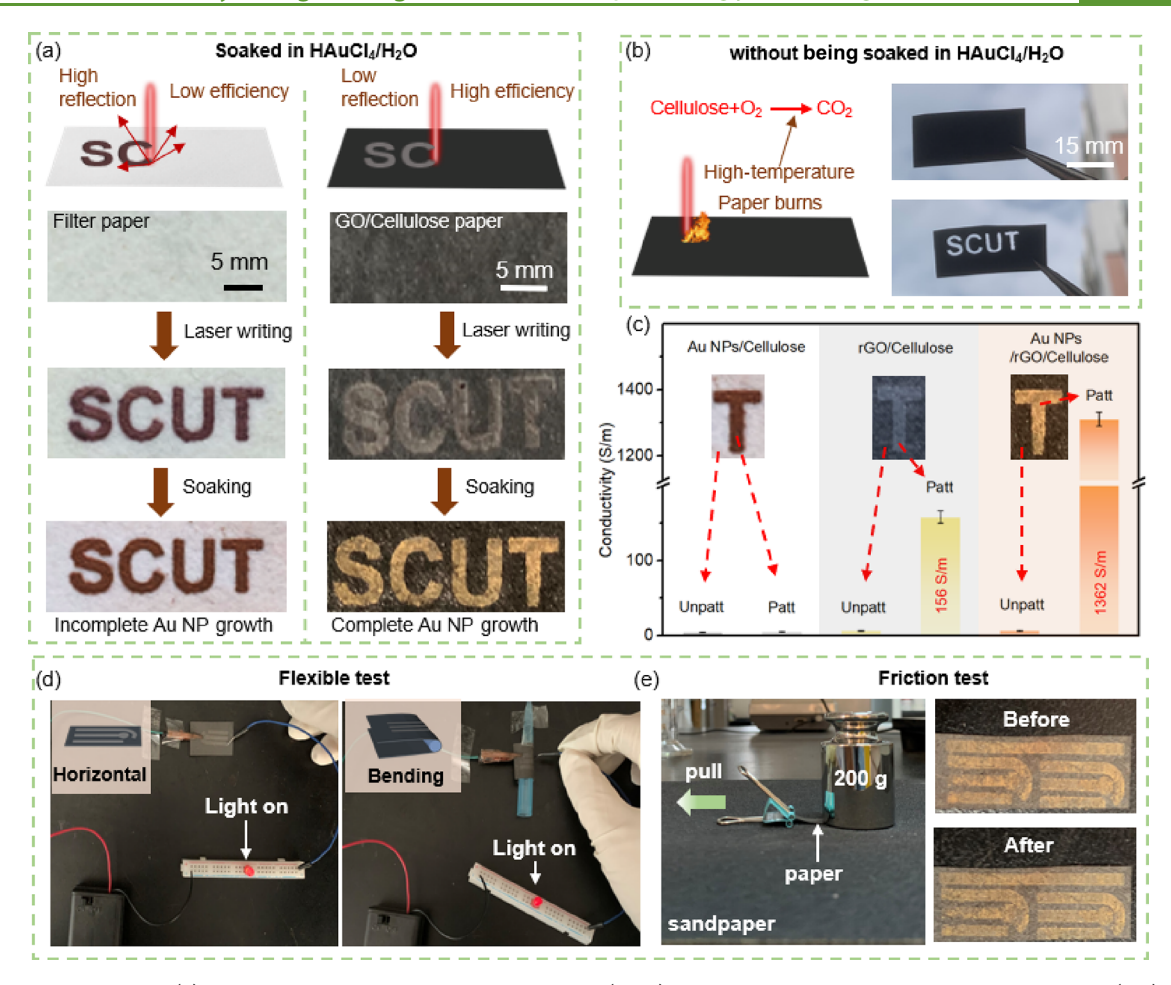


Figure 4. Laser patterning. (a) Patterning of the GO/cellulose composite (right) is more efficient than patterning of filter paper (left). (b) Laser patterning of dry paper burns the GO/cellulose composite. (c) Patterning confers functionality (i.e., conductivity) to the composite. The patterned composite is stable in the (d) flexibility test and (e) friction test.

expected, the O-depleted and Au-enriched regions are colocalized.

Macroscopic Characterization of Laser Patterning. To further illustrate the spatial selectivity of laser patterning, we programmed our system to write four English letters (SCUT) onto paper that had been soaked in HAuCl<sub>4</sub> solution (the laser writing speed is 20 s·cm<sup>-2</sup>, with line widths of ~200  $\mu$ m and a gap of  $\sim$ 40  $\mu$ m). As a control, we first wrote this pattern on filter paper (without GO), as illustrated at the left in Figure 4a. Initial studies showed that laser writing on filter paper was inefficient presumably because the white filter paper reflects most of the laser energy leading to low photothermal heating.<sup>39</sup> In the specimen at the left in Figure 4a, we repeated laser writing five times over the same area and observed the appearance of the red-colored "SCUT" pattern presumably due to the thermal decomposition of HAuCl<sub>4</sub>. For nanoparticle growth on the seeded filter paper, we placed the specimen in 1% HAuCl<sub>4</sub> solution containing hydroxylammonium chloride (0.2%), a reducing agent, for 30 min. After NP growth, the color of the letters on the filter paper changed from deep red to bright red. Importantly, the unpatterned regions showed little color change, indicating that Au NP growth is spatially confined to the laser-induced pre-seeded region.

The right side of Figure 4a illustrates the patterning of the GO/cellulose composite paper that had been soaked in HAuCl<sub>4</sub> solution prior to laser irradiation. The images show that the patterned region became bright gold in color after the

NP growth step. Compared to patterning on filter paper, laser patterning of the black composite paper is more efficient for two reasons. First, patterning only required the laser to pass over the surface once (vs five times for the white filter paper) presumably because the composite absorbs the laser energy more efficiently to yield a higher temperature. Second, growth of Au NP on the pre-seeded region was rapid without requiring an added reducing agent since the rGO appears to catalyze the decomposition of HAuCl<sub>4</sub> into Au NPs (as suggested by the UPS results in Figure S3).

To illustrate the importance of soaking the composite paper before laser writing, we laser irradiated a dry GO/cellulose specimen. Figure 4b illustrates that laser irradiation resulted in such a high temperature that the dry cellulose substrate was burned. While an oxygen-free inert environment may avoid such damage, such a requirement would be less practical for large-scale fabrication. Presumably, the residual aqueous solution in the wet paper serves to limit such extreme temperature excursions.

In addition to altering the chemical structure and visual appearance, laser writing also alters the functional properties (i.e., conductivity) of the paper. To demonstrate this functional patterning, we prepared specimens from cellulose and GO/cellulose papers and measured the conductivities of the patterned and unpatterned regions using a standard four-point probe method. Figure 4c shows that when white paper was laser patterned, both the patterned and unpatterned

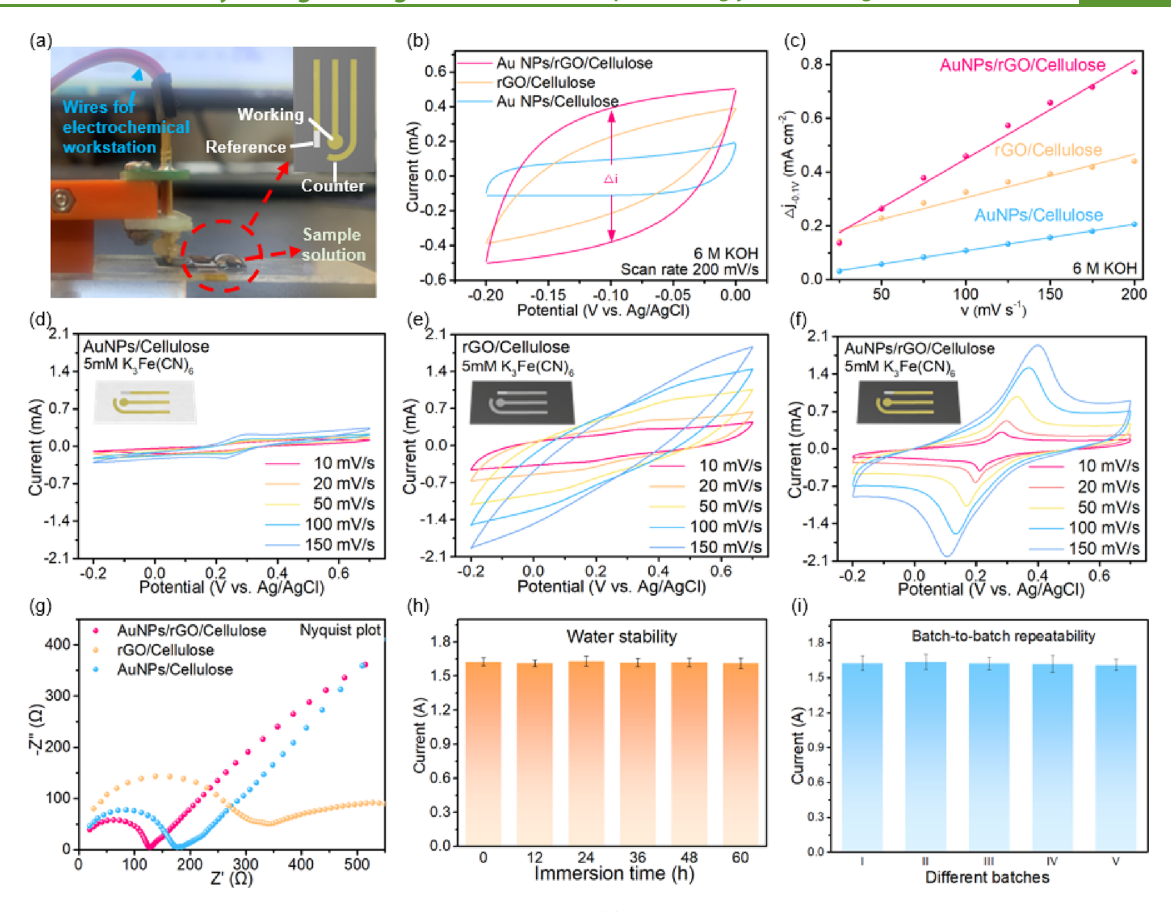


Figure 5. Electrochemical characterization of patterned paper electrodes. (a) Experimental setup for testing a paper-based electrochemical sensor. (b) Cyclic voltammograms of various paper electrodes immersed in KOH solution, where  $\Delta i$  was used as a semi-quantitative estimate of the electrochemically active area. (c) Scan rate studies indicate the AuNPs/rGO/Cellulose electrodes have the highest electrochemically active surface area. Electrochemical measurements using  $K_3Fe(CN)_6$  compare the electro-catalytic activity of patterned electrodes of (d) Au/cellulose; (e) rGO/cellulose; and (f) Au NPs/rGO/cellulose. (g) Electrochemical impedance spectroscopy (EIS) shows that the Au NP/rGO/cellulose paper electrode has the smallest charge transfer resistance. (h) The electrochemical stability of the paper electrode was tested by soaking in water for varying times. (i) Reliability of fabrication was tested by preparing patterned electrodes from various batches of composite paper.

regions remained non-conductive (additional conductivity results are shown in Figure S4). When laser patterning was performed with the GO/cellulose composite without Au, a 25fold difference in conductivity was observed between the patterned (rGO/cellulose; 156 S m<sup>-1</sup>) and unpatterned (GO/ cellulose; 6 S m<sup>-1</sup>) regions. When laser patterning of GO/ cellulose was performed with Au, the conductivity of the patterned region increased after the Au-NP growth step (Au NP/rGO/cellulose; 1362 S m<sup>-1</sup>). Mechanistically, these laserinduced conductivity increases are expected due to the reduction of GO and the formation of a more continuous gold film in the patterned region. Technologically, the important conclusion is that laser patterning of the GO/ cellulose composite allows spatially selective modification with a 200-fold conductivity difference (1362 vs 6 S m<sup>-1</sup>) between the patterned and unpatterned regions.

A more visual illustration of the patterned composite paper's conductivity is shown in Figure 4d. In this demonstration, the patterned paper electrodes were connected in series in the circuit to light a diode. As shown, this diode could be lit when the paper electrode was either flat or folded. The stability of the composite paper was tested by soaking in water to show that the patterned electrode remains intact (Figure S5 of the Supporting Information) and by a friction test. As illustrated in Figure 4e, the friction test was performed by placing the

patterned side of the paper electrode onto sandpaper, adding a 200 g weight onto the surface, and then slowly dragging the paper electrode across the sandpaper. Figure 4e shows that the surface of the paper electrode did not change significantly before and after the friction test, which demonstrates that mechanical stability of the patterned composite paper (the conductivity test of the paper electrode after multiple frictions is shown in Figure S6). Finally, we verify that the patterned paper electrode has good mechanical properties as measured in tensile tests (Figure S7 of the Supporting Information).

Electrochemical Characterization of Patterned Paper Electrodes. To compare the functional properties of various patterned papers, we used the laser to generate a three-electrode pattern for an electrochemical sensor, as illustrated in Figure 5a. One of the electrodes was coated with a Ag/AgCl conductive ink to serve as a reference electrode (RE), while the remaining two patterned regions serve as either the working electrode (WE) or the counter electrode (CE). To prepare a Au NP/cellulose paper with sufficient conductivity for comparison, we laser patterned cellulose paper five times and then performed NP growth steps seven times (Figure S4 shows how conductivity increases with each NP growth step for the cellulose paper).

We first compared the electrochemical active surface area of the paper electrodes by performing CV at various scan rates in

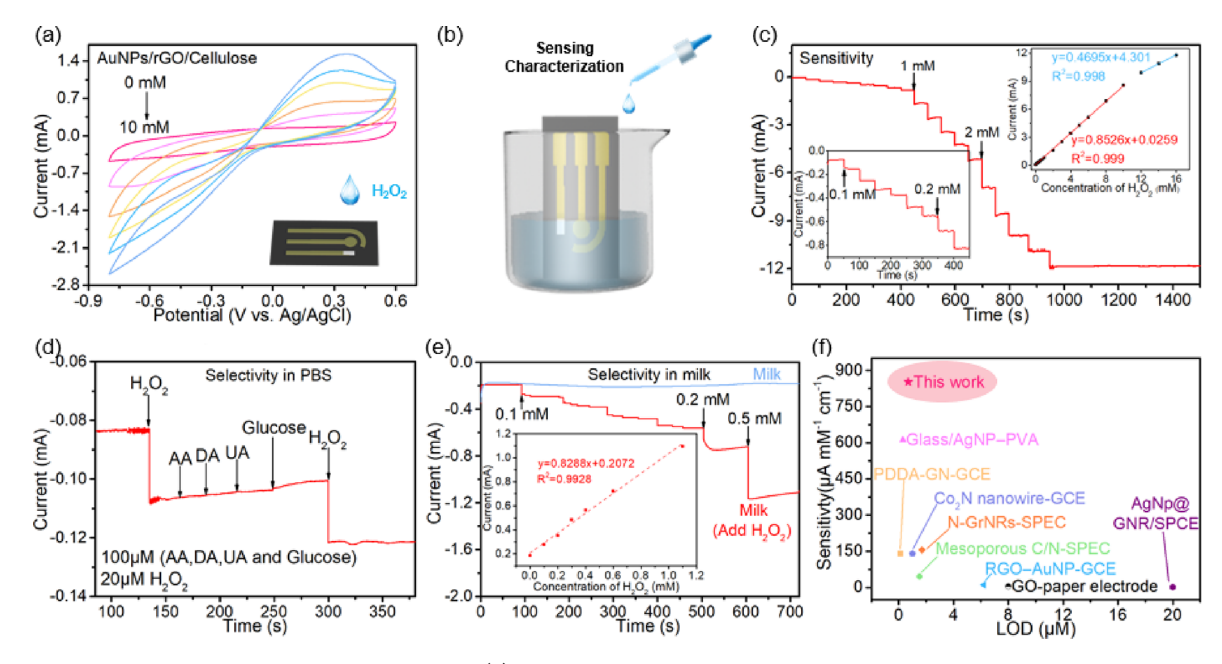


Figure 6. Electrochemical detection by a paper electrode. (a) Demonstration of  $H_2O_2$  detection from a drop using the paper-based electrode. (b) Experimental setup to perform more standard electrochemical characterization. (c) The sensitivity of the response to the  $H_2O_2$  concentration was measured by chronoamperometry (i-t), and the inset at the top right shows the standard curve between current and  $H_2O_2$  concentration. Selectivity was assessed using (d) common interfering compounds and (e) a complex background matrix (i.e., milk). (f) Comparison of the performance of our paper-based electrode for  $H_2O_2$  detection (LOD is the limit of detection).

aqueous potassium hydroxide (6 M; see Figure S8 for further details). The CVs in Figure Sb show results for a scan rate of 200 mV s<sup>-1</sup> (potential range -0.2-0 V) and illustrates that the double-layer capacitance current ( $\Delta i$ ) is obtained by calculating the current difference at a potential of -0.1 V. Figure 5b shows that the patterned cellulose paper without GO (Au NPs/cellulose) has a low  $\Delta i$  (0.20 mA); the patterned composite without Au (rGO/cellulose) has an intermediate  $\Delta i$  (0.45 mA); and the patterned composite with both GO and Au (Au NPs/rGO/cellulose) has a high  $\Delta i$  (0.76 mA).

The active surface area is generally estimated from a linear fit of the double-layer capacitance current as a function of scan rate. Figure 5c shows a good linear fit for our observed  $\Delta i$  values for our three patterned papers: the patterned cellulose paper without GO (Au NPs/cellulose) has the lowest slope; the patterned composite without Au (rGO/cellulose) has an intermediate slope; and the patterned composite with both GO and Au (Au NPs/rGO/cellulose) has the highest slope. These results indicate that the laser-patterned composite with both rGO and Au NPs has an increased conducting surface area.

To compare the electrochemical activities of our paper-based electrodes, we performed CV measurements from a drop of solution containing 5 mM potassium ferricyanide ( $K_3$ Fe-(CN)<sub>6</sub>). Figure 5d shows that the patterned cellulose paper without GO (Au NPs/cellulose) has small current peaks at potentials near the redox potential of  $K_3$ Fe(CN)<sub>6</sub>. Figure 5e shows that the patterned composite without Au (rGO/cellulose) has comparatively larger currents but no peaks associated with the oxidation or reduction of  $K_3$ Fe(CN)<sub>6</sub>. Mechanistically, it is interesting to note that this low electrocatalytic activity is consistent with the ratio of D to G Raman peaks (Figure S1), which indicates that the rGO generated by laser irradiation has few defects, which are important to electrocatalytic activity. Figure 5f shows that the patterned composite with both GO and Au (Au NPs/

rGO/cellulose) has high peak currents for the oxidation and reduction of  $K_3Fe(CN)_6$ . These results indicate that the Au NPs give electrocatalytic activity, which is important for sensing, and the carbon is necessary for conductivity. By comparing with the traditional screen-printing electrochemical sensor, Figure 5f shows that the Au NPs/rGO/cellulose paper-based material has better electrochemical sensing performance.

A final electrochemical characterization method was impedance spectroscopy performed using a mixture of 5 mM  $K_3Fe(CN)_6$  and 5 mM  $K_4Fe(CN)_6$ . This method characterizes the conduction of electrons between the mediator and the electrode. 44,45 Figure 5g shows that the semicircular region for the patterned cellulose paper without GO (Au NPs/cellulose) indicates that it has an intermediate charge transfer resistance: Presumably, its comparatively high electrocatalytic activity compensates for its lower conducting surface area. The large semicircular region for the patterned composite without Au (rGO/cellulose) has a larger charge transfer resistance: presumably due to its low electrocatalytic activity. The small semicircular region for the patterned composite with both Au and GO (Au NPs/rGO/Cellulose) indicates that it has the smallest charge transfer resistance presumably because of good conductivity and electrocatalytic activity.

We performed simple demonstration studies to illustrate the stability and reliability of the composite patterned paper (with Au NPs/rGO/cellulose). To demonstrate water stability, we incubated a paper electrode in water for various times and intermittently used these electrodes to perform CV measurements in a solution of  $K_3Fe(CN)_6$  (5 mM). Figure S5 shows that the water remained clear during this incubation, which provides visual evidence that the patterned composite is stable in water. The oxidation peak current from the CV measurements is plotted in Figure 5h and shows good reproducibility, which provides functional evidence for the stability of the

patterned composite. In a separate experiment, we prepared laser-patterned electrodes from separate batches of composite paper and tested their reproducibility using the analogous CV measurements. The peak currents shown in Figure 5i show that the laser-patterned composite can be fabricated with repeatable functional properties.

Au/rGO/Cellulose Paper Electrode for Electrochemical  $H_2O_2$  Sensors. As a proof of concept, we evaluated our paper-based electrode (patterned with Au NPs/rGO/cellulose regions) for the electrochemical analysis using the commonly studied analyte  $H_2O_2$ . In our initial study, we added a drop of  $H_2O_2$ -containing phosphate-buffered solution (PBS, pH 7) to our electrode and performed CV measurements, as shown in Figure 6a. The CV response for one electrode shows a systematic increase in current with liquid drops containing increasing levels of  $H_2O_2$ . This result indicates that the electrodes that were laser-patterned onto the composite paper were functional and could be used for electrochemical detection.

To evaluate the sensitivity and selectivity of our paper-based electrode patterned with Au NP/rGO/cellulose-conducting regions, we immersed the electrode in various solutions, as illustrated in Figure 6b. The sensitivity was evaluated by adding aliquots of a H<sub>2</sub>O<sub>2</sub> solution and measuring the current response by chronoamperometry (i-t) with the working electrode poised to a reducing potential (at -0.25 V vs Ag/ AgCl). Figure 6c shows that with each H<sub>2</sub>O<sub>2</sub> aliquot added, a rapid step-change in current was observed. The inset in Figure 6c shows the linear standard curve for H<sub>2</sub>O<sub>2</sub> concentrations below 10 mM ( $R^2 = 0.999$ ). At higher concentrations (>10 mM), a linear relationship is also observed but with a smaller slope ( $R^2 = 0.998$ ). In the low-concentration region, the slope of the standard curve indicates a sensitivity of 852.6  $\mu$ A mM<sup>-1</sup> cm<sup>-2</sup>, while the limit of detection (LOD; signal to noise of 3) was calculated to be  $6.2 \times 10^{-7}$  M.

The selectivity for  $H_2O_2$  detection by the paper-based electrode was studied in two ways. First, we examined the effects of the commonly studied interfering compounds ascorbic acid (AA), dopamine (DA), uric acid (UA), and glucose. S4,55 Experimentally, we started with a PBS and added  $H_2O_2$  to adjust the solution to 20  $\mu$ M, as illustrated in Figure 6d. After the current response was observed to be stable, we added individual aliquots of the putative interferences (each added to 100  $\mu$ M). Figure 6d shows that negligible changes in current were observed after each addition. A final addition of  $H_2O_2$  shows the expected, rapid step change in current.

Next, we examined selectivity by spiking a complex matrix (i.e., milk) with aliquots of  $H_2O_2$  [Note:  $H_2O_2$  is commonly added as a preservative to milk, and this practice has motivated the development of rapid methods to detect residual  $H_2O_2.$ ] As illustrated in Figure 6e, with each  $H_2O_2$  aliquot added, a rapid step-change in current was observed, while the inset shows a linear standard curve with a slope that is nearly identical to that observed in buffered solutions (i.e., in Figure 6c). These results illustrate that the paper-based electrodes offer appropriate sensitivities and selectivities for electrochemical analysis.

We compared the performance of our patterned paper electrode to other reports using the sensitivity metrics calculated from Figure 6c. Figure 6f shows that the high sensitivity and low limit of detection (LOD) of our patterned paper electrode compare favorably to other reported electrochemical sensors for H<sub>2</sub>O<sub>2</sub> detection. These results demonstrate that conducting regions composed of rGO and Au NPs

can be laser patterned onto the low-conductivity GO/cellulose substrate to generate functional electronic circuits (i.e., patterned electrodes).

## CONCLUSIONS

In summary, we report a potentially scalable method to create patterned electronic paper that starts with a non-conducting GO cellulose composite, and patterns in conducting regions by wet laser direct writing. Specifically, we report (we believe for the first time) that wet laser writing can be used to simultaneously reduce GO and generate metallic gold seeds. Furthermore, we report that the subsequent growth of gold nanoparticles (NPs) is confined to the previously laserpatterned region. This two-step method (laser-patterning and NP-growth) allows the non-conducting GO-cellulose "substrate" to be patterned with conducting regions composed of gold NPs and rGO. We envision that this work is important because it provides a scalable, repeatable, and inexpensive approach for the manufacture of paper-based electronics for a broad range of applications (e.g., ranging from environmentally friendly single-use sensors to self-powered wearable devices). In particular, conventional papermaking is being adapted to generate a robust composite substrate while optical patterning technology is well established in both conventional microfabrication (e.g., photolithography) and additive manufacturing (e.g., laser patterning).

### ASSOCIATED CONTENT

## Supporting Information

The Supporting Information is available free of charge at https://pubs.acs.org/doi/10.1021/acssuschemeng.3c01943.

General representation for the characterization of Raman, SEM, UPS, conductivity, water stability, friction stability, and mechanical properties of the composite paper electrode; cyclic voltammetry studied for the electrochemical activity area of Au NPs/cellulose, rGO/cellulose, and Au NPs/rGO/cellulose paper electrodes (PDF)

## AUTHOR INFORMATION

## **Corresponding Authors**

Gregory F. Payne – Institute for Bioscience and Biotechnology Research (IBBR), University of Maryland, College Park, Maryland 20742, United States; oocid.org/0000-0001-6638-9459; Email: gpayne@umd.edu

Xiaohui Wang — State Key Laboratory of Pulp and Paper Engineering, South China University of Technology (SCUT), Guangzhou, Guangdong 510640, China; orcid.org/0000-0002-3769-2325; Email: fewangxh@scut.edu.cn

## Authors

Cheng Wang – State Key Laboratory of Pulp and Paper Engineering, South China University of Technology (SCUT), Guangzhou, Guangdong 510640, China

Zhiling Zhao — Institute for Bioscience and Biotechnology Research (IBBR), University of Maryland, College Park, Maryland 20742, United States; orcid.org/0000-0003-0186-7215

Rui Wu – State Key Laboratory of Pulp and Paper Engineering, South China University of Technology (SCUT), Guangzhou, Guangdong 510640, China Xiaowen Shi — School of Resource and Environmental Science, Hubei Biomass-Resource Chemistry and Environmental Biotechnology Key Laboratory, Wuhan University, Wuhan 430079, China; Oorcid.org/0000-0001-8294-2920

Complete contact information is available at: https://pubs.acs.org/10.1021/acssuschemeng.3c01943

### **Author Contributions**

X.W. and C.W. conceived and designed the work. C.W. prepared paper electrodes and carried out characterization and electrochemical sensing detection. R.W. and Z.Z. optimized and repeated the experiment. Z.Z., X.S., and G.F.P. analyzed and interpreted the data. All authors discussed the results and commented on the final manuscript. X.W. and G.F.P. supervised the project.

## **Funding**

This work was supported by the National Key Research and Development Program of China (2019YFE0114400) and the United States National Science Foundation (CBET#1932963).

#### Notes

The authors declare no competing financial interest.

### REFERENCES

- (1) Zhao, D.; Zhu, Y.; Cheng, W.; Chen, W.; Wu, Y.; Yu, H. Cellulose-Based Flexible Functional Materials for Emerging Intelligent Electronics. *Adv. Mater.* **2021**, *33*, 2170213.
- (2) Lamas-Ardisana, P. J.; Martínez-Paredes, G.; Orga, L.; Grande, H. J. Glucose Biosensor Based on Disposable Electrochemical Paper-Based Transducers Fully Fabricated by Screen-Printing. *Biosens. Bioelectron.* **2018**, *109*, 8–12.
- (3) Xiao, T.; Huang, J.; Wang, D.; Meng, T.; Yang, X. Au and Au-Based Nanomaterials: Synthesis and Recent Progress in Electrochemical Sensor Applications. *Talanta* **2020**, *206*, No. 120210.
- (4) Terse-Thakoor, T.; Badhulika, S.; Mulchandani, A. Graphene Based Biosensors for Healthcare. J. Mater. Res. 2017, 32, 2905–2929.
- (5) Pal, A.; Cuellar, H. E.; Kuang, R.; Caurin, H. F.; Goswami, D.; Martinez, R. V. Self-Powered, Paper-Based Electrochemical Devices for Sensitive Point-of-Care Testing. *Adv. Mater. Technol.* **2017**, 1700130.
- (6) Otoni, C. G.; Azeredo, H. M. C.; Mattos, B. D.; Beaumont, M.; Correa, D. S.; Rojas, O. J. The Food–Materials Nexus: Next Generation Bioplastics and Advanced Materials from Agri-Food Residues. *Adv. Mater.* **2021**, *33*, 2102520.
- (7) Dutta, S.; Kim, J.; Ide, Y.; Kim, J. H.; Hossain, M. S. A.; Bando, Y.; Yamauchi, Y.; Wu, K. C. W. 3D Network of Cellulose-Based Energy Storage Devices and Related Emerging Applications. *Mater. Horiz.* **2017**, *4*, 522–545.
- (8) Liu, X.; Li, X.; Gao, X.; Ge, L.; Sun, X.; Li, F. A Universal Paper-Based Electrochemical Sensor for Zero-Background Assay of Diverse Biomarkers. *ACS Appl. Mater. Interfaces* **2019**, *11*, 15381.
- (9) Jemmeli, D.; Marcoccio, E.; Moscone, D.; Dridi, C.; Arduini, F. Highly Sensitive Paper-Based Electrochemical Sensor for Reagent Free Detection of Bisphenol A. *Talanta* **2020**, *216*, No. 120924.
- (10) Caratelli, V.; Fillo, S.; D'Amore, N.; Rossetto, O.; Arduini, F. PAPER-BASED Electrochemical Peptide Sensor for on-Site Detection of Botulinum Neurotoxin Serotype a and C. *Biosens. Bioelectron.* **2021**, *50*, No. 113210.
- (11) Pradela-Filho, L. A.; Noviana, E.; Araújo, D. A.; Takeuchi, R. M.; Henry, C. S. Rapid Analysis in Continuous Flow Electrochemical Paper-Based Analytical Devices. *ACS Sens.* **2020**, *5*, 274.
- (12) Shenguang, G.; Kaiqing, W.; Yan, Z.; Mei, Y.; Jinghua, Y. Paper-Based Biosensor Relying on Flower-like Reduced Graphene Guided Enzymatically Deposition of Polyaniline for Pb2+ Detection. *Biosens. Bioelectron.* **2016**, *80*, 215–221.

- (13) Cinti, S.; Minotti, C.; Moscone, D.; Palleschi, G.; Arduini, F. Fully Integrated Ready-to-Use Paper-Based Electrochemical Biosensor to Detect Nerve Agents. *Biosens. Bioelectron.* **2017**, *93*, 46–51.
- (14) Guo, L.; Wu, X.; Liu, L.; Kuang, H.; Xu, C. Gold Nanoparticle-Based Paper Sensor for Simultaneous Detection of 11 Benzimidazoles by One Monoclonal Antibody. *Small* **2018**, 1701782.
- (15) Zhang, X.; Zhi, H.; Zhu, M.; Wang, F.; Feng, L. Electro-chemical/Visual Dual-Readout Aptasensor for Ochratoxin A Detection Integrated into a Miniaturized Paper-Based Analytical Device. *Biosens. Bioelectron.* **2021**, *180*, No. 113146.
- (16) Kim, Y.; Kim, T.; Lee, J.; Choi, Y. S.; Moon, J.; Park, S. Y.; Lee, T. H.; Park, H. K.; Lee, S. A.; Kwon, M. S.; Byun, H. G.; et al. Tailored Graphene Micropatterns by Wafer-Scale Direct Transfer for Flexible Chemical Sensor Platform. *Adv. Mater.* **2021**, *33*, 2004827.
- (17) Chi, X.; Zhang, X.; Li, Z.; Yuan, Z.; Zhu, L.; Zhang, F.; Yang, J. Fabrication of Microfluidic Chips Based on an EHD-Assisted Direct Printing Method. *Sensors* **2020**, *20*, 1559.
- (18) Ko, Y.; Kim, J.; Kim, D.; Kwon, G.; Yamauchi, Y.; You, J. Fabrication of Highly Conductive Porous Cellulose/PEDOT:PSS Nanocomposite Paper via Post-Treatment. *Nanomaterials* **2019**, *9*, 612.
- (19) Kwon, G.; Lee, K.; Jeon, Y.; Jeong, M.; Kim, J.; You, J. Hybrid Nanoarchitectonics with Conductive Polymer-Coated Regenerated Cellulose Fibers for Green Electronics. *ACS Sustainable Chem. Eng.* **2022**, *10*, 13444–13452.
- (20) Cao, D.; Sun, X.; Wang, Y.; Zhu, H. Bipolar Stackings High Voltage and High Cell Level Energy Density Sulfide Based All-Solid-State Batteries. *Energy Storage Mater.* **2022**, *48*, 458–465.
- (21) Li, Z.; Ruiz, V.; Mishukova, V.; Wan, Q.; Liu, H.; Xue, H.; Gao, Y.; Cao, G.; Li, Y.; Zhuang, X.; Weissenrieder, J.; Cheng, S.; Li, J. Inkjet Printed Disposable High-Rate On-Paper Microsupercapacitors. *Adv. Funct. Mater.* **2022**, 32, 2108773.
- (22) Wang, Y.; Yan, C.; Cheng, S. Y.; Xu, Z. Q.; Sun, X.; Xu, Y. H.; Chen, J. J.; Jiang, Z.; Liang, K.; Feng, Z. S. Flexible RFID Tag Metal Antenna on Paper-Based Substrate by Inkjet Printing Technology. *Adv. Funct. Mater.* **2019**, 29, 1902579.
- (23) Kim, H.; Tran, M. V.; Petryayeva, E.; Solodova, O.; Algar, W. R. Affinity Immobilization of Semiconductor Quantum Dots and Metal Nanoparticles on Cellulose Paper Substrates. *ACS Appl. Mater. Interfaces* **2020**, *12*, 53462–53474.
- (24) Medeiros, M.; Chanci, D.; Martinez, R. V. Moisture-Insensitive, Self-Powered Paper-Based Flexible Electronics. *Nano Energy* **2020**, *78*, No. 105301.
- (25) Zhang, F.; Ren, P.; Guo, H.; Zhang, Z.; Guo, Z.; Dai, Z.; Lu, Z.; Jin, Y.; Ren, F. Flexible and Conductive Cellulose Composite Paper for Highly Efficient Electromagnetic Interference Shielding. *Adv. Electron. Mater.* **2021**, *7*, 2100496.
- (26) Oh, H.; Kwak, S. S.; Kim, B.; Han, E.; Lim, G. H.; Kim, S. W.; Lim, B. Highly Conductive Ferroelectric Cellulose Composite Papers for Efficient Triboelectric Nanogenerators. *Adv. Funct. Mater.* **2019**, 29, 1904066.
- (27) Hou, M.; Xu, M.; Li, B. Enhanced Electrical Conductivity of Cellulose Nanofiber/Graphene Composite Paper with a Sandwich Structure. ACS Sustainable Chem. Eng. 2018, 6, 2983.
- (28) Gao, K.; Shao, Z.; Xue, W.; Wang, X.; Li, J.; Zhang, Y.; Wang, F. Cellulose Nanofibers/Reduced Graphene Oxide Flexible Transparent Conductive Paper. *Carbohydr. Polym.* **2013**, *97*, 243–251.
- (29) Kim, D.; Kim, J.; Henzie, J.; Ko, Y.; Lim, H.; Kwon, G.; Na, J.; Kim, H. J.; Yamauchi, Y.; You, J. Mesoporous Au Films Assembled on Flexible Cellulose Nanopaper as High-Performance SERS Substrates. *Chem. Eng. J.* **2021**, *419*, No. 129445.
- (30) Wang, C.; Wu, R.; Ling, H.; Zhao, Z. L.; Han, W.; Shi, X.; Payne, G. F.; Wang, X. Toward Scalable Fabrication of Electrochemical Paper Sensor without Surface Functionalization. *npj Flexible Electron.* **2022**, *6* (12), 1–8.
- (31) Chen, Y.; Hung, S. F.; Lo, W. K.; Chen, Y.; Shen, Y.; Kafenda, K.; Su, J.; Xia, K.; Yang, S. A Universal Method for Depositing Patterned Materials in Situ. *Nat. Commun.* **2020**, *11*, 5334.

- (32) Shin, D.; Kim, H. R.; Hong, B. H. Gold Nanoparticle-Mediated Noncovalent Functionalization of Graphene for Field-Effect Transistor. *Nanoscale Adv.* **2021**, *3*, 1404.
- (33) Kong, B. S.; Geng, J.; Jung, H. T. Layer-by-Layer Assembly of Graphene and Gold Nanoparticles by Vacuum Filtration and Spontaneous Reduction of Gold Ions. *Chem. Commun.* **2009**, *16*, 2174–2176.
- (34) Yola, M. L.; Atar, N. Amperometric Galectin-3 Immunosensor-Based Gold Nanoparticle-Functionalized Graphitic Carbon Nitride Nanosheets and Core—Shell Ti-MOF@COFs Composites. *Nanoscale* **2020**, *12*, 19824—19832.
- (35) Lee, J. E.; Jang, Y. J.; Xu, W.; Feng, Z.; Park, H. Y.; Kim, J. Y.; Kim, D. H. PtFe Nanoparticles Supported on Electroactive Au–PANI Core@shell Nanoparticles for High Performance Bifunctional Electrocatalysis. *J. Mater. Chem. A* **2017**, *5*, 13692.
- (36) Li, R. Z.; Peng, R.; Kihm, K. D.; Bai, S.; Bridges, D.; Tumuluri, U.; Wu, Z.; Zhang, T.; Compagnini, G.; Feng, Z.; Hu, A. High-Rate in-Plane Micro-Supercapacitors Scribed onto Photo Paper Using in Situ Femtolaser-Reduced Graphene Oxide/Au Nanoparticle Micro-electrodes. *Energy Environ. Sci.* **2016**, *9*, 1458–1467.
- (37) Burrows, N. D.; Harvey, S.; Idesis, F. A.; Murphy, C. J. Understanding the Seed-Mediated Growth of Gold Nanorods through a Fractional Factorial Design of Experiments. *Langmuir* **2017**, 33, 1891–1907.
- (38) Millstone, J. E.; Métraux, G. S.; Mirkin, C. A. Controlling the Edge Length of Gold Nanoprisms via a Seed-Mediated Approach. *Adv. Funct. Mater.* **2006**, *16*, 1209–1214.
- (39) Gischkat, T.; Schachtler, D.; Stevanovic, I.; Balogh-Michels, Z.; Botha, R.; Bächli, A.; Cucinelli, M.; Mocker, A.; Gutsche, M.; Günther, S.; Alder, P.; Eiermann, B. Substrate Cleaning Processes and Their Influence on the Laser Resistance of Anti-Reflective Coatings. *Appl. Sci.* **2020**, *10*, 8496.
- (40) Rabbow, T. J.; Whitehead, A. H. Deconvolution of Electrochemical Double Layer Capacitance between Fractions of Active and Total Surface Area of Graphite Felts. *Carbon* **2017**, *111*, 782–788.
- (41) Li, X.; Shen, J.; Wu, C.; Wu, K. Ball-Mill-Exfoliated Graphene: Tunable Electrochemistry and Phenol Sensing. *Small* **2019**, *15*, 1805567.
- (42) Wei, P.; Shen, J.; Wu, K.; Yang, N. Defect-Dependent Electrochemistry of Exfoliated Graphene Layers. *Carbon* **2019**, *154*, 125–131.
- (43) Zheng, L.; Liu, Y.; Zhang, C. A Sample-to-Answer, Wearable Cloth-Based Electrochemical Sensor (WCECS) for Point-of-Care Detection of Glucose in Sweat. *Sens. Actuators, B* **2021**, 343, No. 130131.
- (44) Randviir, E. P. A Cross Examination of Electron Transfer Rate Constants for Carbon Screen-Printed Electrodes Using Electrochemical Impedance Spectroscopy and Cyclic Voltammetry. *Electrochim. Acta* 2018, 286, 179–186.
- (45) Monnappa, A. B.; Manjunatha, J. G.; Bhatt, A. S. Design of a Sensitive and Selective Voltammetric Sensor Based on a Cationic Surfactant-Modified Carbon Paste Electrode for the Determination of Alloxan. ACS Omega 2020, 5, 23481–23490.
- (46) Murphy, M.; Theyagarajan, K.; Ganesan, P.; Senthilkumar, S.; Thenmozhi, K. Electrochemical Biosensor for the Detection of Hydrogen Peroxide Using Cytochrome c Covalently Immobilized on Carboxyl Functionalized Ionic Liquid/Multiwalled Carbon Nanotube Hybrid. *Appl. Surf. Sci.* **2019**, *492*, 718.
- (47) Sánchez-Calvo, A.; Costa-García, A.; Blanco-López, M. D. C. Paper-Based Electrodes Modified with Cobalt Phthalocyanine Colloid for the Determination of Hydrogen Peroxide and Glucose. *Analyst* **2020**, 2716.
- (48) Stanković, V.; Đurđić, S.; Ognjanović, M.; Mutić, J.; Kalcher, K.; Stanković, D. M. A Novel Nonenzymatic Hydrogen Peroxide Amperometric Sensor Based on AgNp@GNR Nanocomposites Modified Screen-Printed Carbon Electrode. *J. Electroanal. Chem.* **2020**, 876.
- (49) Liu, Y. Y.; Guo, X. L.; Zhao, L.; Zhu, L.; Chen, Z. T.; Chen, J.; Zhang, Y.; Sun, L. T.; Zhao, Y. H. Facile Preparation of Surfactant-

- Free Au NPs/RGO/Ni Foam for Degradation of 4-Nitrophenol and Detection of Hydrogen Peroxide. *Nanotechnology* **2018**, *29*, 235706.
- (50) Xie, F.; Cao, X.; Qu, F.; Asiri, A. M.; Sun, X. Cobalt Nitride Nanowire Array as an Efficient Electrochemical Sensor for Glucose and H<sub>2</sub>O<sub>2</sub> Detection. *Sens. Actuators, B* **2018**, 255, 1254–1261.
- (51) Shi, L.; Niu, X.; Liu, T.; Zhao, H.; Lan, M. Electrocatalytic Sensing of Hydrogen Peroxide Using a Screen Printed Carbon Electrode Modified with Nitrogen-Doped Graphene Nanoribbons. *Microchim. Acta* **2015**, *182*, 2485–2493.
- (52) Arora, P.; Sindhu, A.; Dilbaghi, N.; Chaudhury, A. Engineered Multifunctional Nanowires as Novel Biosensing Tools for Highly Sensitive Detection. *Appl. Nanosci.* **2013**, *3*, 363–372.
- (53) Yan, H.; Wu, Y.; Luo, X.; Jiao, L.; Zhu, C.; Du, D. Tuning Polyelectrolyte-Graphene Interaction for Enhanced Electrochemical Non-Enzymatic Hydrogen Peroxide Sensing. *Anal. Chim. Acta* **2019**, 1049, 98–104.
- (54) Yu, Y.; Peng, J.; Pan, M.; Ming, Y.; Li, Y.; Yuan, L.; Liu, Q.; Han, R.; Hao, Y.; Yang, Y.; Hu, D.; Li, H.; Qian, Z. A Nonenzymatic Hydrogen Peroxide Electrochemical Sensing and Application in Cancer Diagnosis. *Small. Methods* **2021**, 2001212.
- (55) Cernat, A.; Petica, A.; Anastasoaie, V.; Lazar, O.; Györfi, S. J.; Irimes, M.-B.; Stefan, G.; Tertis, M.; Enachescu, M.; Anicăi, L.; Cristea, C. Detection of Hydrogen Peroxide Involving Bismuth Nanowires via Template-Free Electrochemical Synthesis Using Deep Eutectic Solvents. *Electrochem. Commun.* 2020, 121, No. 106869.